Algebraic non-equilibrium wall-stress modelling for large eddy simulation based on analytical integration of the thin boundary-layer equation

Algebraic non-equilibrium wall-stress modeling for large eddy simulation based on analytical integration of the thin boundary-layer equation

Kazuhiko Suga (iD), Tomoki Sakamoto, and Yusuke Kuwata

View Online   **Export Citation**   **CrossMark**

ARTICLES YOU MAY BE INTERESTED IN

Lift force acting on a pair of clean bubbles rising in-line
Physics of Fluids **31**, 072105 (2019); https://doi.org/10.1063/1.5100183

An improved dynamic non-equilibrium wall-model for large eddy simulation
Physics of Fluids **26**, 015108 (2014); https://doi.org/10.1063/1.4861069

Wall-modeling in large eddy simulation: Length scales, grid resolution, and accuracy
Physics of Fluids **24**, 015105 (2012); https://doi.org/10.1063/1.3678331

Algebraic non-equilibrium wall-stress modeling for large eddy simulation based on analytical integration of the thin boundary-layer equation

View Online   Export Citation   CrossMark

Kazuhiko Suga,[a] [ID] Tomoki Sakamoto, and Yusuke Kuwata

AFFILIATIONS

Department of Mechanical Engineering, Osaka Prefecture University, Osaka 599-8531, Japan

[a]Electronic mail: suga@me.osakafu-u.ac.jp

ABSTRACT

An algebraic nonequilibrium wall-stress model for large eddy simulation is discussed. The ordinary differential equation (ODE) derived from the thin-layer approximated momentum equation, including the temporal, convection, and pressure gradient terms, is considered to form the wall-stress model. Based on the concept of the analytical wall function (AWF) for Reynolds-averaged turbulence models, the profile of the subgrid scale (SGS) eddy viscosity inside the wall-adjacent cells is modeled as a two-segment piecewise linear variations. This simplification makes it possible to analytically integrate the ODE near the wall to algebraically give the wall shear stress as the wall boundary condition for the momentum equation. By applying such integration to the wall-normal velocity component, the methodology to avoid the log-layer mismatch is also presented. Coupled with the standard Smagorinsky model, the proposed SGS-AWF shows good performance in turbulent channel flows at Re_τ = 1000–5000 irrespective of the grid resolutions. This SGS-AWF is also confirmed to be superior to the traditional equilibrium wall-stress model in a turbulent backward-facing step flow.

Published under license by AIP Publishing. https://doi.org/10.1063/1.5099658

I. INTRODUCTION

Owing to the recent development and widespread use of high-performance computing systems, industrial computational fluid dynamics (CFD) engineers are now able to choose large eddy simulation (LES) that spatiotemporally resolves grid scale (GS) eddies for their routine work. However, since physical variables such as velocities significantly change in turbulent boundary layers, we need special care for turbulence simulation. Chapman[1] estimated the required numbers of grid points for LES of turbulent boundary layers with and without wall modeling and emphasized the importance of wall modeling for LES. Choi and Moin[2] revisited this issue and estimated the required numbers (N) of computational grid points for direct numerical simulation (DNS), wall-resolved LES (WRLES), and wall-modeled LES (WMLES) as $N \sim Re^{37/14}$, $N \sim Re^{13/7}$, and $N \sim Re$, respectively. Tsubokura[3] referenced their work and stated that it was impossible to perform LES for full-scale industrial flows such as flows around the whole bodies of road vehicles and urban buildings without wall-modeling even by a

ten-petaflops supercomputer. For this reason, to simulate full-scale industrial turbulent flows, the WMLES is essential even by the near future computing facility.

There are two main categories in the WMLES method such as the hybrid LES/Reynolds-averaged Navier-Stokes (RANS) method[4–6] and the wall-stress model (WSM).[7,8] The hybrid LES/RANS method solves a RANS turbulence model in the near-wall regions that are embedded in the LES domain, while the WSM gives wall boundary conditions to the LES that is applied to the whole flow domain. Since the WSM does not require zoning the computational domain in principle, it makes the simulation algorithm easier, particularly for flows in complex geometries. The most classical and simplest WSM gives the wall shear stress algebraically assuming that the logarithmic law of the velocity[9,10] is valid locally and instantaneously. However, such an assumption is not convinced when it is applied to complex flows.

Accordingly, the majority of the recently practiced WSMs assume the thin boundary-layer equation (TBLE) for the wall-parallel velocity u_i as

$$\frac{\partial u_i}{\partial t} + \frac{\partial u_i u_j}{\partial x_j} + \frac{1}{\rho}\frac{\partial p}{\partial x_i} = \frac{\partial}{\partial y}\left[(\nu + \nu_t)\frac{\partial u_i}{\partial y}\right], \qquad (1)$$

where ρ, p, ν, and ν_t are the fluid density, pressure, kinematic viscosity, and turbulent viscosity, respectively. For the turbulent viscosity, the mixing length model (MLM) with a damping function such as

$$\nu_t/\nu = \kappa y^+[1 - \exp(-y^+/A^+)]^2 \qquad (2)$$

is usually applied.[7,8,11–13] In the above model, κ and A^+ are the von Kármán and model constants, respectively. (Usually, $\kappa = 0.41$ and $A^+ = 17$ are applied.) The wall-normal distance y is normalized by the viscous scale: $y^+ = u_\tau y/\nu$, where u_τ is the friction velocity. Although Eq. (1) includes the temporal, convection, and pressure gradient terms, the most common WSM is the equilibrium model that assumes that the lhs of Eq. (1) is zero. The resultant ordinary differential equation (ODE) is solved using a 1D finite volume method over nonuniformly stretched grids between the wall and the first off-wall node points of the LES mesh.[7]

Although the equilibrium wall-stress modeling is rather simple and robust, there is no question that nonequilibrium wall-stress modeling, which considers some or all of the terms on the lhs of Eq. (1), is potentially more accurate. Hoffmann and Benocci[14] suggested using the pressure gradient and temporal terms for the wall-stress modeling. Wang and Moin[12] systematically examined the effects of retaining the pressure gradient term and all the terms of Eq. (1). They confirmed that the RANS-type eddy viscosity in Eq. (1) should be reduced when the convective terms were retained to account for the unresolved part of the Reynolds stress. For this reason, Cabot and Moin[11] suggested a dynamically adjusted von Kármán constant across the inner layer to match the RANS and LES Reynolds stresses. This practice was followed by Kawai and Larsson[15] and Park and Moin.[16]

As discussed by Kawai and Larsson,[13] modeling the wall stress using the first off-wall grid point LES data often produces the log-layer mismatch (LLM) of the mean velocity profile. Although some earlier studies[17–22] tried to remove it by modifying the subgrid scale (SGS) models, Kawai and Larsson[13] pointed out that it came from the lack of the fine vortex scale information near the walls. Since the near-wall fine vortices are inevitably unresolved in the WMLES, the LES velocities at the first off-wall node points are contaminated by the truncation and SGS modeling errors. Consequently, the integration using such erroneous outer boundary velocities in the WSM produces under- or overestimated wall stresses. Their remedy to this anomaly was to abandon the first off-wall grid point data and use the data at a little more distant matching locations from the wall for the wall-stress modeling.

However, Yang et al.[23] argued that although the Kawai-Larson (K-L) treatment was useful for its robustness, ensuring the proper matching locations was almost impossible at the meshing stage for complex geometries with unstructured elements. Moreover, they commented that the K-L treatment unphysically detached the wall stress from the closest LES velocity, failing to properly account for sharp turning angles or skewed velocity profiles. Correspondingly, Yang et al.[23,24] proposed a local wall-stress model using the time-filtered information taken from the wall-adjacent LES solution to remove the LLM. This method introduces an effective under-relaxation of the velocity used in the wall model.

Although there are several other recent attempts on the wall-stress modeling,[16,25] many of them are not simple enough for implementation and require to set near-wall modeling layers. Moreover, to the best of the authors' knowledge, there has been no recent attempt to develop an algebraic WSM that does not require to embed such near-wall layers. However, when we change our concern to the RANS turbulence modeling, there have been similar attempts to improve the wall functions (WFs). Note that in the RANS society, a WSM is equivalent to a wall function (WF). Since the validity of the logarithmic law becomes ambiguous in complex flows, during the last two decades, several research groups revisited the wall-function approach and attempted to develop new schemes.[26–30] Among them, Craft et al.[26] proposed a new wall-function strategy that integrated the simplified TBLE analytically over the control volumes adjacent to the wall, assuming a near-wall variation of the eddy viscosity. Since it takes account for the convection and pressure gradient terms, it is categorized in the nonequilibrium model. The resulting "algebraic expressions" of the wall shear stress and other quantities are applied to solving the transport equations. This strategy is called the analytical wall function (AWF) and has been improved and extended so that it can be applicable to complex turbulent flow fields.[31–35] For example, the present authors' group extended the range of capability of the model to rough walls[31] and high Prandtl/Schmidt number turbulent scalar fields.[32,34]

Therefore, this study tries to develop an "algebraic" nonequilibrium WSM for LES based on the rich experience of RANS AWFs. We call such an algebraic nonequilibrium model the "SGS-AWF" hereafter. While we develop the SGS-AWF, we have found how to avoid the LLM quite easily, and thus, this paper is organized as follows: in Sec. II, a general description of the numerical scheme and the development of SGS-AWF are given. The model validation in several high Reynolds number turbulent channel flows followed by the validation in a turbulent backward-facing step flow is discussed in Sec. III. Finally, the conclusions are summarized in Sec. IV, followed by the discussion on the LLM in the Appendix.

II. NUMERICAL SCHEMES

The CFD code used in this study is an in-house finite difference solver of three-dimensional incompressible filtered Navier-Stokes equations by the SMAC scheme.[36] It applies the second-order central differencing to the convection, diffusion, and pressure gradient terms on a staggered grid and the second-order Adams-Bashforth method to the temporal term.

A. Large eddy simulation

LES decomposes the turbulent flow into grid scale (GS) eddies that are larger than the grid size and the SGS eddies that are smaller than the grid size by the filtering operator $\langle \cdot \rangle$. The decomposition of u_i is described as

$$u_i = \langle u_i \rangle + \tilde{u}_i, \qquad (3)$$

where $\tilde{u}_i$ is the SGS velocity. The governing equations of the LES for an incompressible flow are thus

$$\frac{\partial \langle u_i \rangle}{\partial x_i} = 0, \qquad (4)$$

$$\frac{\partial \langle u_i \rangle}{\partial t} + \langle u_j \rangle \frac{\partial \langle u_i \rangle}{\partial x_j} = -\frac{1}{\rho}\frac{\partial \langle p \rangle}{\partial x_i} + \frac{\partial}{\partial x_j}\left(\nu \frac{\partial \langle u_i \rangle}{\partial x_j}\right) - \frac{\partial \tau_{ij}}{\partial x_j}, \quad (5)$$

where

$$\tau_{ij} = \langle u_i u_j \rangle - \langle u_i \rangle \langle u_j \rangle. \quad (6)$$

The SGS stress τ_{ij} is modeled by the eddy viscosity model as

$$\tau_{ij} = -2\nu_{sgs}S_{ij} + \frac{2}{3}\delta_{ij}k_{sgs}, \quad (7)$$

where ν_{sgs}, k_{sgs}, and S_{ij} are the SGS eddy viscosity, the SGS turbulence energy, and the strain tensor which is $S_{ij} = \frac{1}{2}\left(\frac{\partial \langle u_i \rangle}{\partial x_j} + \frac{\partial \langle u_j \rangle}{\partial x_i}\right)$. To the turbulent viscosity, the standard Smagorinsky model[37] is applied as

$$\nu_{sgs} = (c_s f_s \Delta)^2 \sqrt{2S_{ij}S_{ji}}, \quad (8)$$

where $f_s = 1 - \exp(-y^+/A_s)$ and $\Delta = (\Delta_1 \Delta_2 \Delta_3)^{1/3}$. The grid spacing in the x_i direction is Δ_i, and the model coefficients applied are $c_s = 0.1$ and $A_s = 25$.

B. Algebraic nonequilibrium wall-stress model: SGS-AWF

TBLE (1) for LES can be rewritten as

$$\frac{\partial}{\partial y}\left[(\nu + \nu_{sgs})\frac{\partial \langle u_i \rangle}{\partial y}\right] = \underbrace{\left[\frac{\partial \langle u_i \rangle}{\partial t} + \frac{\partial \langle u_i \rangle \langle u_j \rangle}{\partial x_j} + \frac{1}{\rho}\frac{\partial \langle p \rangle}{\partial x_i}\right]}_{C_{U_i}}. \quad (9)$$

If the rhs of Eq. (9) can be presumed to be constant in the wall-normal y-direction inside a wall-adjacent cell, this assumption which is a common practice in the finite volume method leads to

$$\frac{\partial}{\partial y}\left[(\nu + \nu_{sgs})\frac{\partial \langle u_i \rangle}{\partial y}\right] = C_{U_i}^P, \quad (10)$$

where the superscript (or subscript) "P" denotes a value at the first off-wall node point P. When the near-wall profile of the SGS eddy viscosity ν_{sgs} is modeled as Eq. (2), one can integrate Eq. (10) as an ordinary differential equation (ODE) to obtain the filtered velocity profile. However, since the mixing length model of Eq. (2) is based on the friction velocity, its reliability becomes ambiguous near stagnation and reattachment points where the friction velocity vanishes.

In the RANS AWF,[26] instead of using the friction velocity, a one-equation-like expression of the eddy viscosity

$$\nu_t = c_\mu \sqrt{k}\ell_\varepsilon \quad (11)$$

was applied. In this form, ν_t, c_μ, ℓ_ε, and k are the eddy viscosity, model constant, dissipation length scale, and turbulent kinetic energy, respectively. Since the dissipation length scale in the boundary layer was modeled[38] as $\ell_\varepsilon = c_\ell y$,

$$\nu_t = c_\mu c_\ell \sqrt{k}y. \quad (12)$$

With the assumption that k does not change drastically in the equilibrium boundary layer, the eddy viscosity may be expressed as

$$\nu_t/\nu \simeq c_\mu c_\ell \sqrt{k^P}y/\nu = \alpha y^*, \quad (13)$$

where $y^* = y\sqrt{k^P}/\nu$ and $\alpha = c_\mu c_\ell$. Accordingly, the RANS AWF introduces the normalized wall-normal distance y^* using the square
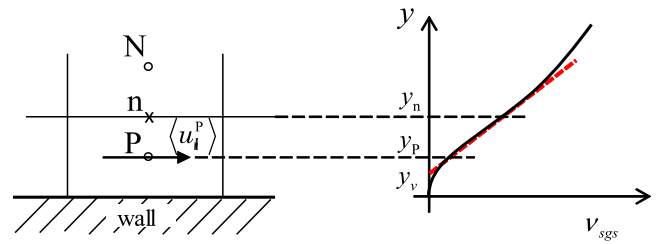

FIG. 1. Near-wall grid arrangement and the SGS eddy viscosity. The solid curve represents the actual distribution profile of ν_{sgs}, while the red dashed line represents the linear assumption. The y-intercept of the red linear dashed line is y_v.

root of turbulent kinetic energy as a velocity scale instead of the friction velocity to avoid anomaly at the stagnation or reattaching points. Then, to consider viscous sublayer effects, instead of introducing a damping function, the profile of ν_t was modeled as

$$\nu_t/\nu = \max[0, \alpha(y^* - y_v^*)], \quad (14)$$

where y_v corresponds to the viscous sublayer thickness. Note that in the equilibrium boundary layer, the relations between ℓ_ε and the mixing length l_m and between y^+ and y^* can be derived[39] as $\ell_\varepsilon \simeq l_m c_\mu^{-3/4}$ and $y^+ \simeq c_\mu^{1/4}y^*$, respectively. Here, the model coefficients chosen were $c_\mu = 0.09$, $c_\ell = 2.55$, and $y_v^* = 10.7$.

Based on the scale similarity assumption between the GS and SGS turbulence, ν_{sgs} may be also modeled as

$$\nu_{sgs} = c_\mu \sqrt{k_{sgs}}\ell_\varepsilon. \quad (15)$$

Then, broadly following the above-described strategy, the profile of the SGS eddy viscosity inside a wall-adjacent cell is modeled as a two-segment piecewise linear variations, as shown in Fig. 1, although the actual profile of the SGS eddy viscosity is not that simple and should depend on the grid size. The equation for such a modeled SGS eddy viscosity profile shown in Fig. 1 can be written as

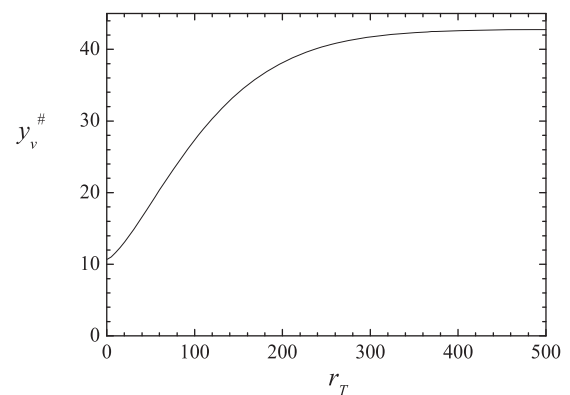$$\nu_{sgs}/\nu = \max[0, \alpha(y^\# - y_v^\#)], \quad (16)$$

FIG. 2. Profile of $y_v^\#$ against the time scale ratio, r_T, of the SGS to GS turbulence.

TABLE I. Geometric parameters of the wall shear stress by Eq. (25).

	D	E
$0 \leq y_\nu \leq y_\mathrm{n}$	$y_\nu^\# + \frac{1}{\alpha}\ln[1 + \alpha(y_\mathrm{n}^\# - y_\nu^\#)]$	$-\frac{y_\mathrm{n}^\# - y_\nu^\#}{\alpha} - \frac{(y_\nu^\#)^2}{2} + \frac{1 - \alpha y_\nu^\#}{\alpha^2}\ln[1 + \alpha(y_\mathrm{n}^\# - y_\nu^\#)]$
$y_\mathrm{n} \leq y_\nu$	$y_\mathrm{n}^\#$	$-\frac{(y_\nu^\#)^2}{2}$

where $y^\# = y\sqrt{k_{sgs}^\mathrm{P}}/\nu$. Since the normalized value $y_\nu^\#$ includes k_{sgs}, it should depend on the grid size and the instantaneous flow situation, and it is no longer a constant. It is also affected by how k_{sgs} is estimated when the standard Smagorinsky model[37] is applied. In this study, following Horiuti,[40] k_{sgs} is estimated by filtering the velocity field as

$$k_{sgs} = C_k \sum_{i=1}^{3} (\langle u_i \rangle - \langle\langle u_i \rangle\rangle)^2, \qquad (17)$$

where $\langle\langle u_i \rangle\rangle$ is the double-filtered velocity and the model constant is $C_k = 1$. The estimation procedure[41] for $\langle\langle u_i \rangle\rangle$ is based on the Simpson method, which is expressed as

$$\langle\langle u_i \rangle\rangle = \frac{1}{2}\langle u_i^\mathrm{P} \rangle + \frac{\langle u_i^\mathrm{E} \rangle + \langle u_i^\mathrm{W} \rangle + \langle u_i^\mathrm{N} \rangle + \langle u_i^\mathrm{S} \rangle + \langle u_i^\mathrm{T} \rangle + \langle u_i^\mathrm{B} \rangle}{12}, \quad (18)$$

where $\langle u_i^\mathrm{E} \rangle$, $\langle u_i^\mathrm{W} \rangle$, ... are the velocities of the neighboring nodes of node P. For the wall-adjacent node P shown in Fig. 1, the present study simply sets as $\langle u_i^\mathrm{S} \rangle = 0$. After nonexhaustive numerical experiments, our empirical attempt has selected the functional profile of $y_\nu^\#$ shown in Fig. 2, whose numerical expression is

$$y_\nu^\# = 10.7\{3[1 - \exp(-r_T/125)^{1.4}] + 1\}, \qquad (19)$$

where r_T is the time scale ratio of the SGS to GS turbulence: $r_T = (k_{sgs}/\varepsilon_{sgs})\sqrt{S_{ij}S_{ji}}$, with $\varepsilon_{sgs} = k_{sgs}^{3/2}/\Delta_y$. Note that the above formula is purely empirically determined. Although Eq. (17) may not necessarily estimate correct values, effects of such incorrectness are considered to be effectively absorbed in the above optimized model function [Eq. (19)].

When ν_{sgs} is described by the linear function of $y^\#$ as in Eq. (16), analytical integration of Eq. (10) can be easily performed, if $y^\# < y_\nu^\#$,

$$\frac{d\langle u_i \rangle}{dy^\#} = (C_{U_i}^{\mathrm{P}\#} y^\# + A_{U_i})/\nu, \qquad (20)$$

$$\langle u_i \rangle = \frac{C_{U_i}^{\mathrm{P}\#}}{2\nu}(y^\#)^2 + \frac{A_{U_i}}{\nu}y^\# + B_{U_i}, \qquad (21)$$

and if $y^\# \geq y_\nu^\#$,

$$\frac{d\langle u_i \rangle}{dy^\#} = \frac{C_{U_i}^{\mathrm{P}\#} y^\# + A_{U_i}'}{\nu\{1 + \alpha(y^\# - y_\nu^\#)\}}, \qquad (22)$$

$$\langle u_i \rangle = \frac{C_{U_i}^{\mathrm{P}\#}}{\alpha\nu}y^\# + \left\{\frac{A_{U_i}'}{\alpha\nu} - \frac{C_{U_i}^{\mathrm{P}\#}}{\alpha^2\nu}(1 - \alpha y_\nu^\#)\right\}\ln[1 + \alpha(y^\# - y_\nu^\#)] + B_{U_i}', \qquad (23)$$

where $C_{U_i}^{\mathrm{P}\#} = (\nu^2/k_{sgs}^\mathrm{P})C_{U_i}^\mathrm{P}$. The integration constants A_{U_i}, B_{U_i}, etc., are determined by applying the nonslip boundary condition at the wall, y_ν, and the cell face point, y_n. The values at y_n are determined by

interpolation between the calculated node values at P and N, while at $y = y_\nu$ a monotonic distribution condition is imposed by ensuring that the velocity gradients should be continuous. Hence, $B_{U_i} = 0$, $A_{U_i}' = A_{U_i}$, and $B_{U_i}' = \frac{C_{U_i}^{\mathrm{P}\#}}{2\nu}(y_\nu^\#)^2 + \frac{A_{U_i}}{\nu}y_\nu^\# - \frac{C_{U_i}^{\mathrm{P}\#}}{\alpha\nu}y_\nu^\#$ are obtained for the nonslip wall boundary.

The result is that the wall shear stress can be expressed as

$$\tau_{wi} = \mu\frac{d\langle u_i \rangle}{dy}\bigg|_{wall} = \mu\frac{\sqrt{k_{sgs}^\mathrm{P}}}{\nu}\frac{d\langle u_i \rangle}{dy^\#}\bigg|_{wall} = \rho\frac{\sqrt{k_{sgs}^\mathrm{P}}}{\nu}A_{U_i}, \qquad (24)$$

where μ is the fluid dynamic viscosity. Accordingly, what we need is A_{U_i}, which is calculated as

$$A_{U_i} = \frac{\nu\langle u_i^\mathrm{n} \rangle + C_{U_i}^{\mathrm{P}\#}E}{D}. \qquad (25)$$

The geometric parameters D and E are listed in Table I. As discussed above, from the velocity gradient obtained by the integration of the TBLE inside the wall-adjacent cell, the role of the SGS-AWF is to provide the wall stress which is apparently correlated with the molecular viscosity. However, once the wall stress is given by the SGS-AWF, the molecular viscosity in Eq. (5) may not be necessary for LES applications in atmospheric boundary layers and ocean mixed layers where the molecular viscosity effect is negligible.

The important tip is that Eqs. (20) and (22) are also applied to the boundary condition for the wall-normal velocity component $\langle u_2 \rangle$ which is located at $y = y_\mathrm{P}$ in the staggered grid arrangement as

$$\frac{d\langle u_2 \rangle}{dy}\bigg|_{y_\mathrm{P}} = (C_{U_2}^{\mathrm{P}\#}y_\mathrm{P}^\# + A_{U_2})\sqrt{k_{sgs}^\mathrm{P}} \;\; \times \nu^{-2}, \;\; \text{if } y_\mathrm{P}^\# < y_\nu^\# \qquad (26)$$

$$= \frac{(C_{U_2}^{\mathrm{P}\#}y_\mathrm{P}^\# + A_{U_2})\sqrt{k_{sgs}^\mathrm{P}}}{\nu^2\{1 + \alpha(y^\# - y_\nu^\#)\}}, \;\; \text{if } y_\mathrm{P}^\# \geq y_\nu^\#. \qquad (27)$$

Note that to give the above equations (24), (26), and (27), the nonslip/nonpenetration wall condition is used. However, those resultant wall-stress boundary conditions are the Neumann-type conditions and do not necessarily impose the solutions to be nonslip/nonpenetration at the wall. The WSM gives equivalent wall stresses to those of nonslip/nonpenetration wall boundaries. In such a case, the nonpenetration condition is imposed by the wall-normal convection at the wall.

III. MODEL VALIDATION

A. Turbulent channel flows

For the turbulent channel flows, as shown in Fig. 3, the computational domain of $4\pi\delta(x) \times 2\delta(y) \times 2\pi\delta(z)$ is applied. The calculated cases are for the friction Reynolds numbers $Re_\tau = (u_\tau\delta)/\nu = 1000$,
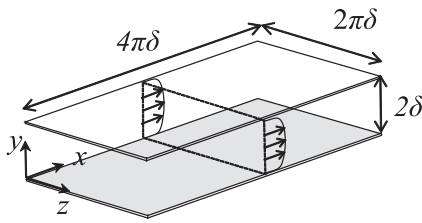
FIG. 3. Computational domain of the turbulent channel flows.

TABLE II. Grid spacing for turbulent channel flows.

Re_τ	NY = 20			NY = 40			NY = 60		
	Δ_x^+	Δ_y^+	Δ_z^+	Δ_x^+	Δ_y^+	Δ_z^+	Δ_x^+	Δ_y^+	Δ_z^+
1000	102	100	51	102	50	51	102	34	51
2000	203	200	102	203	100	102	203	67	102
4000	406	400	203	406	200	203	406	133	203
5000	508	500	254	508	250	254	508	166	254

2000, 4000, and 5000 based on the channel half height δ and the friction velocity. The periodic boundary condition is applied to the streamwise and spanwise directions. The number of cells distributed uniformly in the x- and z-directions is 126. Regarding the number of cells in the y-direction, three cases of NY = 20, 40, and 60, which correspond to the number of cells distributed uniformly across the channel height, are tested to evaluate the mesh dependency of the wall model. In Table II, the resolutions of the cases are listed. Note that these mesh resolutions for the LES are significantly coarse. The results processed during more than ten turnover times are compared with the DNS data for each Reynolds number case.

Figure 4(a) compares the mean velocity profiles by the SGS-AWF and the DNS of Bernardini et al.[42] at Re_τ = 2000. The SGS-AWF integrates the ODE (10) between the wall and the cell face "n" shown in Fig. 1. Correspondingly, the red dashed line indicates the obtained velocity profile by the resultant Eqs. (21) and (23). One can see good agreement between the DNS result and the profile by the integration of the ODE. This confirms that the assumption in the

SGS-AWF is quite reasonable and the velocity field that is used to assume the wall shear stress, Eq. (24), is reliable. With such a wall stress, the LES velocity profile shown with symbols agrees well with the DNS profile.[42] For a wide range of Reynolds numbers, Fig. 4(b) compares the mean velocity profiles by the SGS-AWF and the DNS profile. From Re_τ = 1000 to 5000, irrespective of Re_τ, it is confirmed that the velocity profiles produced by the SGS-AWF agree well with the DNS profile. To see the insensitivity to the grid resolution, Figs. 5(a) and 5(b) compare the results by three different grid resolutions at Re_τ = 2000 and 4000, respectively. It can be confirmed that the SGS-AWF can produce reasonably insensitive results to the grid resolutions.

The notable thing in the above discussion is that although the plots by the SGS-AWF sometimes slightly deviate from the log-law line, one cannot see obvious LLM in Figs. 4 and 5. We have found that this is mainly from the application of Eqs. (26) and (27) to the boundary condition of the wall-normal velocity component. The slight offsets with the initial points come from the assumption of the two-segment distributions for the eddy viscosity shown in Fig. 1. If one chooses continuous profile of the eddy viscosity like the MLM, Eq. (2), such offsets are removed. The details of these points are discussed in the Appendix using the MLM.

Figures 6(a) and 6(b) compare the presently obtained resolved root mean square (rms) velocity fluctuations and the DNS data[42] at Re_τ = 2000 and 4000. Since the grid spacing is large, the resolved rms velocity fluctuations are not enough to evaluate the Reynolds stresses. This is common, particularly for the WMLES. Indeed, such a trend was also seen in previous studies. In the report of Cabot and Moin,[11] the general trend of the rms velocity fluctuations in a turbulent channel flow looked quite similar to that shown in Figs. 6(a) and 6(b). Their spanwise and wall-normal rms velocity fluctuations by a nonequilibrium WSM coupled with the dynamic SGS model were generally lower and became significantly lower than those of the resolved LES. For the streamwise component, the rms value rose toward the wall and suddenly dropped at the first off-wall grid point like in this study. Chung and Pullin[43] also indicated the near-wall drop of the streamwise component by their WSM for their stretched vortex SGS. Similar near-wall kinks have been also seen in some other studies.[13,25] To make up the difference between the GS components and the reference data, the SGS components need considering. However, it is impossible for the Smagorinsky-type SGS model since k_{sgs} in Eq. (7) is not explicitly calculated. As seen in
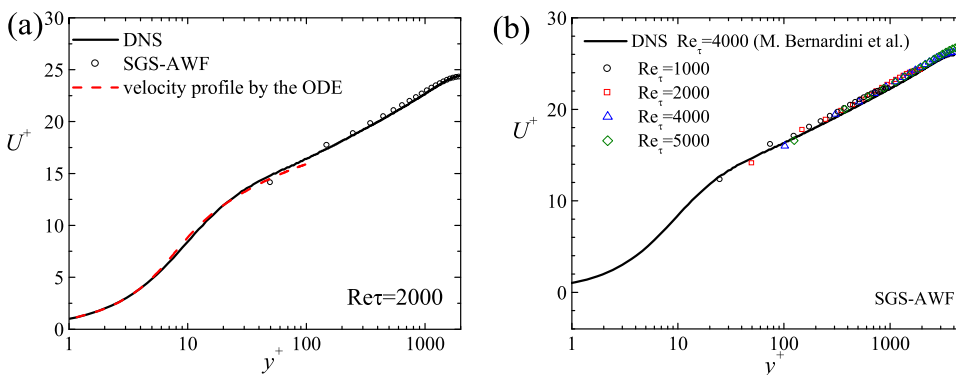

FIG. 4. Streamwise mean velocity profiles by the SGS-AWF: (a) velocity profiles at Re_τ = 2000 with the ODE solution and (b) velocity profiles at different Reynolds numbers. Grid resolution is NY = 40.
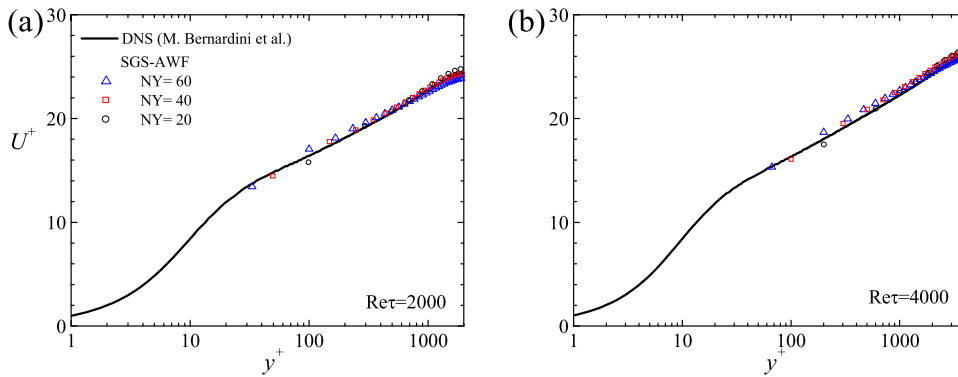
FIG. 5. Streamwise mean velocity profiles by the SGS-AWF with different grid resolutions: at (a) Re_τ = 2000 and (b) Re_τ = 4000.

Figs. 6(c) and 6(d), the contribution from the SGS part becomes significant toward the wall and becomes comparable with the GS component. Hence, the near-wall decrease of the resolved rms values takes place. Note that the SGS component can be correctly evaluated for the shear stress. Furthermore, the distribution of the normalized anisotropic Reynolds stress tensor $[a_{ij} = 2\overline{u'_i u'_j}/\overline{u'_k u'_k} - (2/3)\delta_{ij}]$ shown in Fig. 7 indicates that the behaviour toward the wall does not show such a steep drop for any normal component, a_{ii}. Correspondingly, although the steep drop in the streamwise rms component may look curious, we consider that it is simply from the wall boundary.

For the Reynolds shear stress, the SGS and molecular stresses are also plotted along with the resolved GS stress in Figs. 6(c) and 6(d). We see that although the resolved GS stress is rather smaller

near the wall for both Re_τ cases, the agreement between the DNS data and the GS plus SGS stresses becomes satisfactory. The linear profile of the total stress (the sum of the GS, SGS, and molecular stresses) corresponds to the fully developed velocity field in the channel.

B. Backward-facing step flow

The backward-facing step is a typical flow geometry for separating, recirculating, and reattaching flows. These typical flow characteristics can be seen in numerous engineering applications, such as flows around buildings, inside combustors, etc. Hence, it is very important to investigate the performance of the WSM in such a geometry. The main feature of the backward-facing step flow is
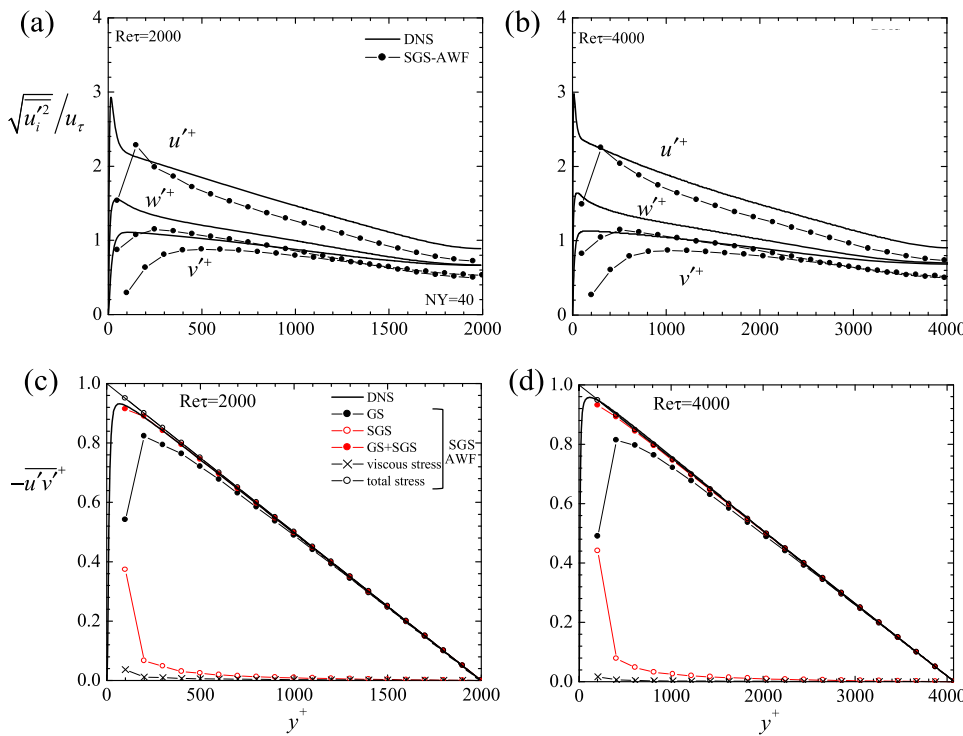

FIG. 6. Resolved velocity fluctuations and Reynolds stress profiles in turbulent channel flows by the SGS-AWF: (a) rms velocities at Re_τ = 2000, (b) rms velocities at Re_τ = 4000, (c) shear stresses at Re_τ = 2000, and (d) shear stresses at Re_τ = 4000. Grid resolution is NY = 40.
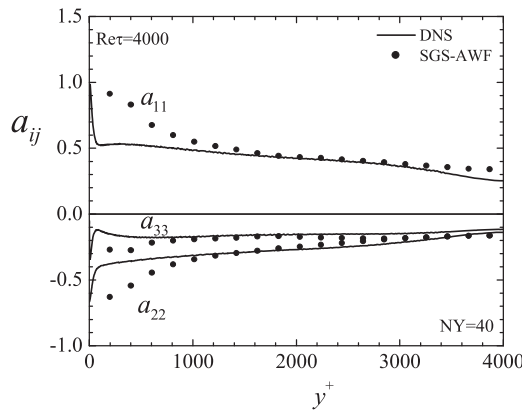
FIG. 7. Resolved anisotropic Reynolds stress profiles in turbulent channel flows by the SGS-AWF at $Re_\tau = 4000$. $a_{ij} = 2\overline{u'_i u'_j}/\overline{u'_k u'_k} - (2/3)\delta_{ij}$. Grid resolution is NY = 40.

TABLE III. Grid resolution for turbulent backward-facing step flow.

	Δ_y/H	Δ_x/H	Δ_z/H
Grid 1	0.10	0.07–1.16	0.20
Grid 2	0.067	0.07–1.16	0.20

The origin of the coordinate system is located at the bottom of the step. The spanwise length of the computational domain is set as $2\pi H$, which is longer than that recommended by Le[46] in which $4H$ was adequate to tail the two-point correlations for u, v, and w near the wall. The size of the computational domain in the streamwise direction is $56H$ ($6H$ for the upstream region of the step, while $50H$ for the downstream region). To investigate the mesh dependency, two kinds of grids are used. The numbers of grid points for each grid are $212(x) \times 50(y) \times 63(z)$ and $212(x) \times 75(y) \times 63(z)$, respectively, for Grid 1 and Grid 2. The grid resolution is summarized in Table III. Note that uniform spacings are applied in the y- and z-directions, while nonuniform spacings are used for the x-direction. The statistical results are obtained by processing the data for ten turnover times.

The predicted reattachment length by the SGS-AWF is $X_R/H = 6.7$, while the modified MLM (mMLM) predicts $X_R/H = 6.8$ with both grids. (Compared with Grid 1, the predicted values of X_R/H with Grid 2 become slightly shorter.) Here, the mMLM is a version of the MLM with the modified wall-normal boundary treatment discussed in the Appendix. As shown in the Appendix, the mMLM does not produce the LLM at all. Although both WSMs show good accuracy for predicting the recirculation as the experimental

that due to the sudden expansion of the geometry, the flow separates from the step edge forming a shear layer and eventually reattaches to the bottom surface. The case simulated consists of a flow inside a channel with a one-sided sudden expansion, with the expansion ratio $E_R = 1.25$. Figure 8 shows an overview of the geometry. The Reynolds number $Re = U_C H/\nu$, based on the step height H and the inlet mean centerline velocity U_C, is set as 28 000. The expansion ratio and the Reynolds number correspond to those of the classical experiments conducted by Vogel and Eaton.[44] Cabot and Moin[11] also simulated this backward-facing step flow and they applied WSMs only to the bottom wall after the step, while this study applies the WSM to all wall boundaries. For the inlet boundary condition, an auxiliary simulation of a periodic turbulent channel flow is conducted and velocity and pressure data on a vertical plane are extracted and used to define time-dependent Dirichlet boundary conditions at the inlet plane. As the outlet boundary condition, the Sommerfeld radiation condition[45]

$$\frac{\partial \phi}{\partial t} + C \frac{\partial \phi}{\partial x} = 0 \qquad (28)$$

is applied at the outlet plane, where C in Eq. (28) is the "convection velocity of vortex structures." The bulk velocity at the outlet plane is used as the convection velocity of vortex structures in this study. The periodic boundary condition is used for the spanwise boundary condition. As for the coordinate axes, x, y, and z indicate the streamwise, vertical, and spanwise directions, respectively.
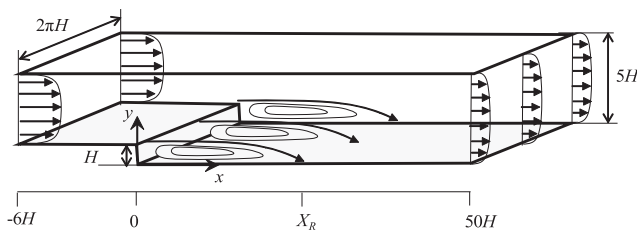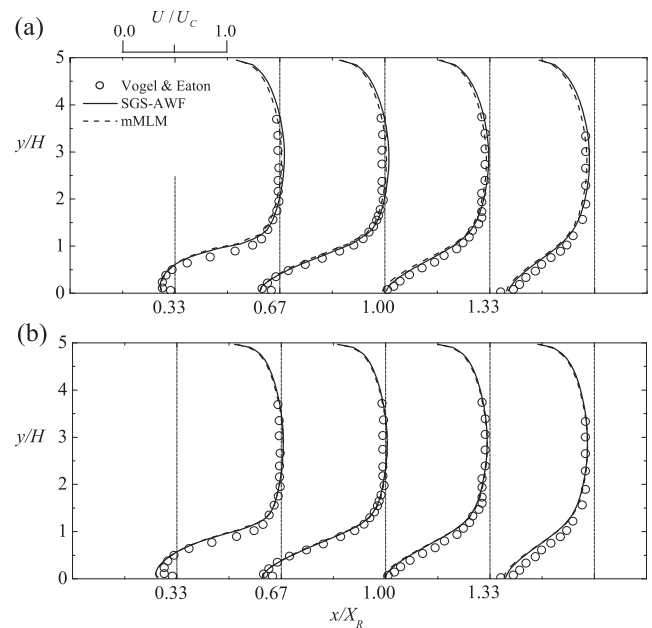

FIG. 8. Computational domain of the turbulent backward-facing step flow.

FIG. 9. Comparison of mean velocities of the turbulent backward-facing step flow: (a) by Grid 1 and (b) by Grid 2.
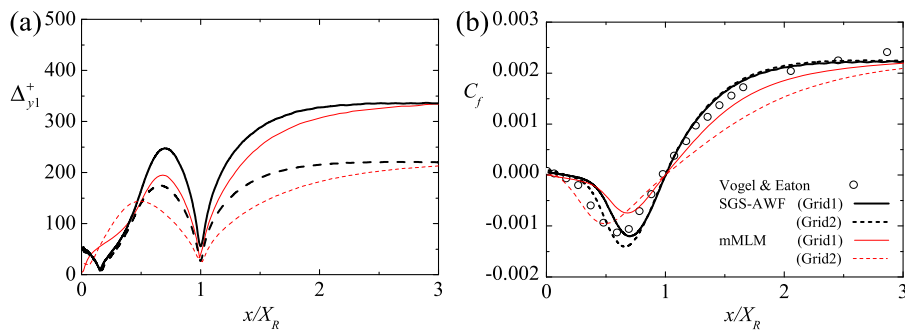
FIG. 10. Comparison of wall-normal cell heights and the friction coefficients: (a) distribution of the normalized wall-normal cell heights and (b) distribution of the friction coefficients.

reattachment length[44] was X_R/H = 6.7, the SGS-AWF produces slightly better results than the mMLM.

Figure 9 compares the streamwise mean velocity profiles by the SGS-AWF and the mMLM. It is seen that the discrepancies between the two WSMs are very slight, and irrespective of the grid resolutions, both models predict virtually the same velocity profiles which agree well with the experimental data. When we look at the normalized sizes of the wall-adjacent cells Δ_{y1}^+ in Fig. 10(a), the difference in the grid resolutions of two grids is large. This implies that the general flow field predicted by those WSMs seems not very sensitive to the wall-normal grid resolution. However, the reverse flow at x/X_R = 0.33 is slightly overpredicted with Grid 2. The similar trend is seen in the previous LES by Rouhi and Piomelli.[47] They also predicted a little stronger reverse flow than the experiments with a similar wall-normal grid resolution.

Although the improvement of predicting the recirculation is not very large to claim the superiority of the SGS-AWF, the profile of the friction coefficient $C_f = 2\tau_w/(\rho U_C^2)$ by the SGS-AWF is clearly better than that by the mMLM as shown in Fig. 10(b). While the mMLM underestimates the overall friction coefficient, the SGS-AWF shows better agreement with the experimental data by both grid resolutions. Since the SGS-AWF is a nonequilibrium WSM considering the influence of the pressure gradient, convection, and time derivative terms, it can represent better wall stresses under the presence of large pressure gradients after the step. These results are consistent with those reported by Cabot and Moin[11] who compared the equilibrium and nonequilibrium WSMs. Another good point with the SGS-AWF is that its grid dependency on the prediction looks much milder than that of the mMLM. Indeed, as the change in the grid resolution (Grid 1 → Grid 2), the predicted C_f by the mMLM changes significantly, while the SGS-AWF produces nearly the same profiles.

IV. CONCLUSIONS

A new algebraic nonequilibrium wall-stress model for large eddy simulation is developed. Based on the concept of the analytical wall function for Reynolds-averaged turbulence models, the profile of the subgrid scale eddy viscosity inside the wall-adjacent cells is modeled as a two-segment piecewise linear variation. By this simplification, analytical integration of the ordinary differential equation that is the thin-layer approximated momentum equation, which includes the temporal, convection, and pressure gradient

terms, is performed over the wall-adjacent cells to give the wall shear stress algebraically as the wall boundary condition for the momentum equation. The model coefficient of this SGS-AWF is expressed dynamically with the time scale ratio of the SGS to GS motions. By applying the same strategy to the wall-normal direction, it is shown that the log-layer mismatch can be suppressed. This implies that the main reason for the log-layer mismatch is the inconsistent boundary treatment between the wall-parallel and wall-normal velocity components. Coupled with the standard Smagorinsky model, the proposed SGS-AWF shows good performance in turbulent channel flows at Re_τ = 1000–5000 irrespective of the grid resolutions. The SGS-AWF is also confirmed to be better and less grid sensitive than the traditional equilibrium wall-stress model in a turbulent backward-facing step flow where nonequilibrium flow effects are important.

APPENDIX: REMEDY FOR THE LOG-LAYER MISMATCH

As discussed by Kawai and Larsson,[13] modeling the wall stress using the wall-adjacent node point produces the LLM of the mean velocity profile due to the lack of the fine vortex scale information near the walls. Since the near-wall fine vortices are inevitably unresolved in the WMLES, they claimed that the near-wall LES velocities were contaminated by the truncation and SGS modeling errors, and thus, the integration using such erroneous outer boundary velocities produced inaccurate wall stresses. In fact, Fig. 11(a) shows the LLM in the mean velocities of turbulent channel flows reproduced by the MLM, Eq. (2), in the equilibrium WSM. Although the first off-wall grid points are reasonably on the log-law line, clear LLM can be seen from the second off-wall grid points at any Reynolds number.

The scheme of the standard equilibrium WSM may be reviewed below. With the eddy viscosity, Eq. (2), to obtain the wall shear stress
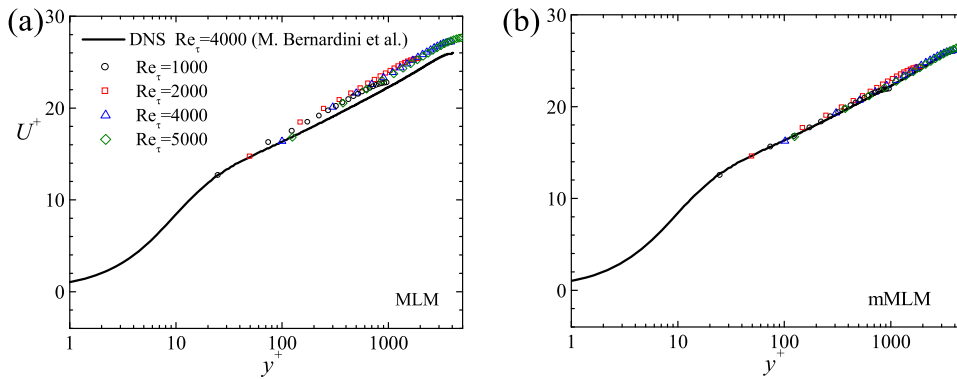
FIG. 11. Streamwise mean velocity distribution by the mixing length-based WSM: (a) LLM profiles by the standard equilibrium WSM and (b) corrected profiles by the modified scheme. Grid resolution is NY = 40. Note that Kawai-Larsson's treatment[13] is not applied. The values at all node points are plotted.

for the wall-parallel velocity components, we integrate

$$\frac{\partial}{\partial y}\left[(v + v_t)\frac{\partial \langle u_i \rangle}{\partial y}\right] = 0 \quad (A1)$$

from the wall to the cell face "n" shown in Fig. 1. Although to integrate the above one-dimensional ODE, the finite difference/volume method on a submesh embedded into the wall-adjacent cell may be usually applied with the wall boundary condition, we apply an alternative scheme as follows. With the integration constant C_i, the integrated form of Eq. (A1) is

$$[\langle u_i \rangle]_0^{y_n} = \int_0^{y_n} \frac{C_i}{(v + v_t)} dy. \quad (A2)$$

When the nonslip wall boundary condition is applied, the integration constant can be obtained as

$$C_i = \frac{\langle u_i^n \rangle}{\int_0^{y_n} \frac{dy}{v + v_t}}. \quad (A3)$$

If the denominator of Eq. (A3) cannot be analytically integrated, one may apply the numerical integration using the trapezoidal rule on the submesh. In this study, for example, we applied a 1D submesh embedded between the wall and cell face n with nonuniformly distributed 200 nodes. By applying the obtained integration constant

C_i, one can give the boundary condition as a Neumann boundary condition for the velocity $\langle u_i \rangle$ at the wall as

$$\left.\frac{d\langle u_i \rangle}{dy}\right|_{wall} = \left.\frac{C_i}{(v + v_t)}\right|_{wall}, \quad (A4)$$

which is related to the wall shear stress when $\langle u_i \rangle$ is the wall-parallel velocity. However, to calculate the wall-normal velocity component of the LES part, the nonpenetration boundary condition $\langle u_2 \rangle = 0$ is simply applied to the central difference in the diffusion terms.

During the present study, we have found that when one also applies Eq. (A4) as the boundary condition for $\langle u_2 \rangle$ at y_P,

$$\left.\frac{d\langle u_2 \rangle}{dy}\right|_{y_P} = \left.\frac{C_2}{(v + v_t)}\right|_{y_P}, \quad (A5)$$

the LLM is totally suppressed, as shown in Fig. 11(b). Note that although the nonpenetration condition at the wall is used to obtain the integration constant C_2, the WSM itself does not necessarily impose the solution to satisfy the nonpenetration wall condition. It gives the wall stresses that are equivalent to those at the nonpenetration wall. (The nonpenetration condition is imposed by the wall-normal convection at the wall.) The MLM with this treatment is called the modified MLM (mMLM). Compared with the SGS-AWF in Fig. 4(b), the velocity plots by the mMLM in Fig. 11(b) beautifully
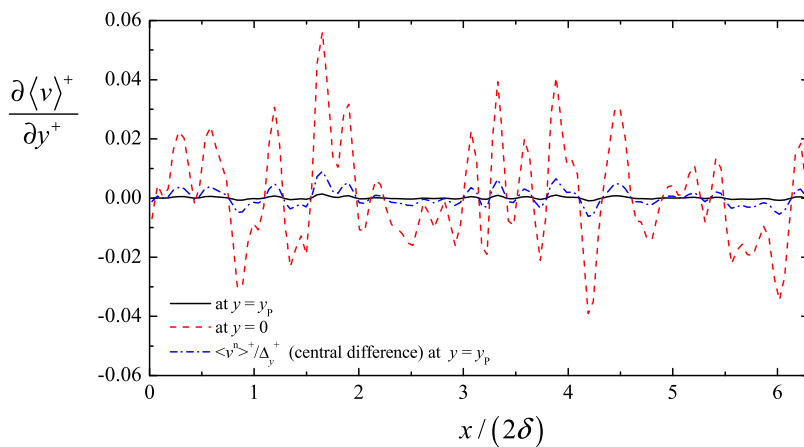

FIG. 12. Instantaneous distribution of the near-wall gradient of the wall-normal velocity component in the central plane by Eqs. (A4) and (A5) at $Re_\tau = 4000$.
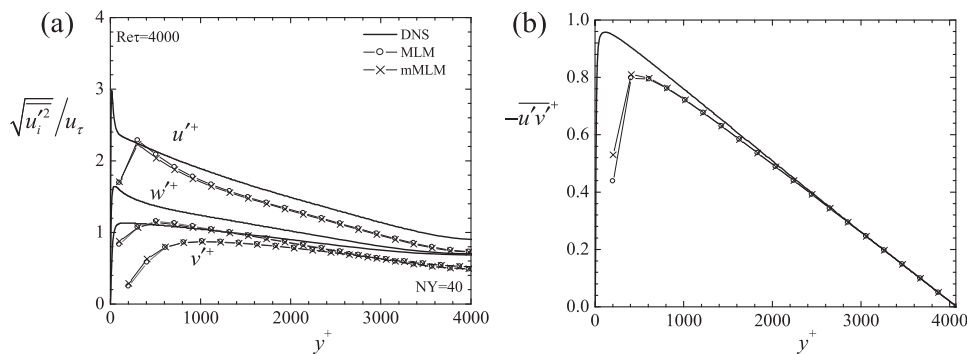
FIG. 13. Comparison of resolved velocity fluctuations and Reynolds stress profiles in turbulent channel flows: (a) rms velocities at $Re_\tau = 4000$ and (b) shear stresses at $Re_\tau = 4000$. Grid resolution is NY = 40.

collapse on the log-law line. This may be because the MLM, Eq. (2), is a continuous single function, while the eddy viscosity of the SGS-AWF, Eq. (16), is a two-segment function.

As pointed out by Bae *et al.*,[25] since the "filtered velocity" is different from the unfiltered velocity, the filtered wall-normal velocity and its gradient at the wall are not necessarily zero instantaneously. Moreover, from the continuity, although the nonslip wall condition requires $\frac{d\langle u_2 \rangle}{dy}\Big|_{wall} = 0$, $\langle u_1 \rangle = \langle u_3 \rangle = 0$ at the wall is not always the case by the WSM as commented above. Accordingly, as shown in Fig. 12, $\frac{d\langle v \rangle}{dy}$ by Eq. (A4) has nonzero instantaneous values at the wall. Figure 12 also shows the significant difference between the levels of $\frac{d\langle v \rangle}{dy}\Big|_{y_P}$ by Eq. (A5) and by the central difference. Hence, we see that the central difference with $\langle v \rangle = 0$ does not necessarily produce a reliable value. This implies that the main reason for the LLM is the inconsistent boundary treatment between the wall-parallel and wall-normal velocity components.

Figure 13 compares the resolved rms velocity fluctuations and Reynolds shear stress profiles by the MLM and mMLM. It is clear that the proposed LLM free boundary treatment does not contribute to improve those profiles significantly.

REFERENCES

[1] D. R. Chapman, "Computational aerodynamics development and outlook," AIAA J. **17**, 1293–1313 (1979).

[2] H. Choi and P. Moin, "Grid-point requirements for large eddy simulation: Chapman's estimates revisited," Phys. Fluids **24**, 011702 (2012).

[3] M. Tsubokura, "Applied aerodynamics simulation for the next generation based on the massively parallel CFD: From the K-computer to the post-K," Nagare **35**, 77–85 (2016).

[4] U. Piomelli, "Wall-layer models for large eddy simulations," Prog. Aerosp. Sci. **44**, 437 (2008).

[5] P. R. Spalart, "Detached-eddy simulation," Annu. Rev. Fluid Mech. **41**, 181–202 (2009).

[6] C. Mockett, M. Fuchs, and F. Thiele, "Progress in DES for wall-modelled LES of complex internal flows," Comput. Fluids **65**, 44–55 (2012).

[7] J. Larsson, S. Kawai, J. Bodart, and I. Bermejo-Moreno, "Large eddy simulation with modeled wall-stress: Recent progress and future directions," Mech. Eng. Rev. **3**, 15–00418 (2016).

[8] S. T. Bose and G. I. Park, "Wall-modeled large-eddy simulation for complex turbulent flows," Annu. Rev. Fluid Mech. **50**, 535–561 (2018).

[9] D. Spalding, "A single formula for the law of the wall," J. Appl. Mech. **28**, 455–458 (1961).

[10] A. J. Musker, "Explicit expression for the smooth wall velocity distribution in a turbulent boundary layer," AIAA J. **17**, 655–657 (1979).

[11] W. Cabot and P. Moin, "Approximate wall boundary condition in the large-eddy simulation of high Reynolds number flow," Flow, Turbul. Combust. **63**, 269–291 (1999).

[12] M. Wang and P. Moin, "Dynamic wall modeling for large-eddy simulation of complex turbulent flows," Phys. Fluids **14**, 2043–2051 (2002).

[13] S. Kawai and J. Larsson, "Wall-modeling in large eddy simulation: Length scales, grid resolution, and accuracy," Phys. Fluids **24**, 015105 (2012).

[14] G. Hoffmann and C. Benocci, "Approximate wall boundary conditions for large eddy simulations," in *Advances in Turbulence V*, edited by R. Benzi (Springer, Berlin, 1995), pp. 222–228.

[15] S. Kawai and J. Larsson, "Dynamic non-equilibrium wall-modeling for large eddy simulation at high Reynolds numbers," Phys. Fluids **25**, 015105 (2013).

[16] G. I. Park and P. Moin, "An improved dynamic non-equilibrium wall-model for large eddy simulation," Phys. Fluids **26**, 015108 (2014).

[17] F. K. Chow, R. L. Street, M. Xue, and J. H. Ferziger, "Explicit filtering and reconstruction turbulence modeling for large-eddy simulation of neutral boundary layer flow," J. Atmos. Sci. **62**, 2058 (2005).

[18] F. Ding, S. P. Arya, and Y.-L. Lin, "Large-eddy simulations of the atmospheric boundary layer using a new subgrid-scale model-I. Slightly unstable and neutral cases," Environ. Fluid Mech. **1**, 29 (2001).

[19] E. Lévêque, F. Toschi, L. Shao, and J.-P. Bertoglio, "Shear-improved Smagorinsky model for large-eddy simulation of wall-bounded turbulent flows," J. Fluid Mech. **570**, 491 (2007).

[20] F. Porté-Agel, C. Meneveau, and M. B. Parlange, "A scale-dependent dynamic model for large-eddy simulation: Application to a neutral atmospheric boundary layer," J. Fluid Mech. **415**, 261 (2000).

[21] P. P. Sullivan, J. C. McWilliams, and C.-H. Moeng, "A subgrid-scale model for large-eddy simulation of planetary boundary-layer flows," Boundary Layer Meteorol. **71**, 247 (1994).

[22] J. A. Templeton, G. Medic, and G. Kalitzin, "An eddy-viscosity based near-wall treatment for coarse grid large-eddy simulation," Phys. Fluids **17**, 105101 (2005).

[23] X. I. A. Yang, G. I. Park, and P. Moin, "Log-layer mismatch and modeling of the fluctuating wall stress in wall-modeled large-eddy simulations," Phys. Rev. Fluids **2**, 104601 (2017).

[24] X. I. A. Yang, J. Sadique, R. Mittal, and C. Meneveau, "Integral wall model for large eddy simulations of wall-bounded turbulent flows," Phys. Fluids **27**, 025112 (2015).

[25] H. J. Bae, A. Lozano-Durán, S. T. Bose, and P. Moin, "Dynamic slip wall model for large-eddy simulation," J. Fluid Mech. **859**, 400–432 (2019).

[26] T. Craft, A. Gerasimov, H. Iacovides, and B. Launder, "Progress in the generalization of wall-function treatments," Int. J. Heat Fluid Flow **23**, 148–160 (2002).

[27] T. Craft, S. Gant, H. Iacovides, and B. Launder, "A new wall function strategy for complex turbulent flows," Numer. Heat Transfer, Part B **45**, 301–318 (2004).

[28] T. Knopp, T. Alrutz, and D. Schwamborn, "A grid and flow adaptive wall-function method for RANS turbulence modelling," J. Comput. Phys. **220**, 19–40 (2006).

[29] M. Popovac and K. Hanjalić, "Compound wall treatment for RANS computation of complex turbulent flows and heat transfer," Flow, Turbul. Combust. **78**, 177–202 (2007).

[30] S. V. Utyuzhnikov, "Robin-type wall functions and their numerical implementation," Appl. Numer. Math. **58**, 1521–1533 (2008).

[31] K. Suga, T. Craft, and H. Iacovides, "An analytical wall-function for turbulent flows and heat transfer over rough walls," Int. J. Heat Fluid Flow **27**, 852–866 (2006).

[32] K. Suga, "Computation of high Prandtl number turbulent thermal fields by the analytical wall-function," Int. J. Heat Mass Transfer **50**, 4967–4974 (2007).

[33] K. Suga and S. Nishiguchi, "Computation of turbulent flows over porous/fluid interfaces," Fluid Dyn. Res. **41**, 012401 (2009).

[34] K. Suga and M. Kubo, "Modeling turbulent high Schmidt number mass transfer across undeformable gas-liquid interfaces," Int. J. Heat Mass Transfer **53**, 2989–2995 (2010).

[35] K. Suga, Y. Ishibashi, and Y. Kuwata, "An analytical wall-function for recirculating and impinging turbulent heat transfer," Int. J. Heat Fluid Flow **41**, 45–54 (2013).

[36] A. A. Amsden and F. H. Harlow, "A simplified MAC technique for incompressible fluid flow calculations," J. Comput. Phys. **6**, 322–325 (1970).

[37] J. Smagorinsky, "General circulation experiments with the primitive equations: I. The basic experiment," Mon. Weather Rev. **91**, 99–164 (1963).

[38] B. E. Launder and D. B. Spalding, "The numerical computation of turbulent flows," Comput. Methods Appl. Mech. Eng. **3**, 269–289 (1974).

[39] B. E. Launder and D. B. Spalding, *Mathematical Models of Turbulence* (Academic Press, London, UK, 1972).

[40] K. Horiuti, "A proper velocity scale for modeling subgrid-scale eddy viscosities in large eddy simulation," Phys. Fluids A **5**, 146–157 (1993).

[41] M. Inagaki, M. Nagaoka, N. Horiuchi, and K. Suga, "Large eddy simulation analysis of engine steady intake flows using a mixed-time-scale subgrid-scale model," Int. J. Engine Res. **11**, 229–241 (2010).

[42] M. Bernardini, S. Pirozzoli, and P. Orlandi, "Velocity statistics in turbulent channel flow up to $re_\tau = 4000$," J. Fluid Mech. **742**, 171–191 (2014).

[43] D. Chung and D. I. Pullin, "Large-eddy simulation and wall modelling of turbulent channel flow," J. Fluid Mech. **631**, 281–309 (2009).

[44] J. C. Vogel and J. K. Eaton, "Combined heat transfer and fluid dynamic measurements downstream of a backward-facing step," J. Heat Transfer **107**, 922–929 (1985).

[45] A. Sommerfeld, *Partial Differential Equations in Physics* (Academic Press, New York, 1949).

[46] H. Le, "Direct numerical simulation of turbulent flow over a backward-facing step," Ph.D. dissertation (Stanford University, California, USA, 1995).

[47] A. Rouhi, U. Piomelli, and B. J. Geurts, "Dynamic subfilter-scale stress model for large-eddy simulations," Phys. Rev. Fluids **1**, 044401 (2016).